

Article

Magnetotelluric-Geochemistry Investigations of Blawan Geothermal Field, East Java, Indonesia

Sukir Maryanto ^{1,2,*}, Cinantya N. Dewi ¹, Vanisa Syahra ^{1,2}, Arief Rachmansyah ³, James H. Foster ⁴, Ahmad Nadhir ^{1,2} and Didik R. Santoso ^{1,2}

¹ Department of Physics, Faculty of Sciences, Universitas Brawijaya, Veteran Street, Malang 65145, Indonesia; cinanthiiia@gmail.com (C.N.D.); vanisa.syahra@gmail.com (V.S.); anadhir@ub.ac.id (A.N.); dieks@ub.ac.id (D.R.S.)

² Center of Energy and Natural Resources, Institute of Research and Community Services, Universitas Brawijaya, Veteran Street, Malang 65145, Indonesia

³ Department of Civil Engineering, Faculty of Engineering, Universitas Brawijaya, MT Haryono Street, Malang 65145, Indonesia; ariefftub@ub.ac.id

⁴ Hawaii Institute of Geophysics and Planetary, University of Hawaii, 1680 East-West Road, Pacific Ocean Science & Technology (POST) Building, Room 602 Honolulu, HI 96822, USA; jamesfos@hawaii.edu

* Correspondence: sukir@ub.ac.id; Tel.: +62-813-211-57868

Academic Editors: Maurizio Barbieri and Jesús Martínez Frías

Received: 26 March 2017; Accepted: 24 May 2017; Published: 10 June 2017

Abstract: An integrated magnetotelluric (MT) and geochemical study of the Blawan geothermal field has been performed. The character of the hot springs, the reservoir temperature, and geothermal reserve potential of Blawan geothermal field are assessed. MT measurements, with 250 m up to 1200 m spacings, were made at 19 sites, and 6 locations at the Blawan hot springs have been sampled for geochemical survey. The results of 2D modelling indicated that the geothermal system in the research area consisted of a cap rock zone ($\leq 32 \Omega \cdot \text{m}$), reservoir zone ($> 32 - \leq 512 \Omega \cdot \text{m}$), and heat source zone ($> 512 \Omega \cdot \text{m}$), and also identified faults. The characteristics of the hot spring water were identified through analyzing the major and minor elements. A ternary diagram (Cl-SO₄-HCO₃) showed that the Blawan hot springs consist of bicarbonate water (at locations of AP-01, AP-02, AP-03) and chloride water (at locations of AP-04, AP-05, and AP-06), with a reservoir temperature of approximately 90 °C based on the Na-K-Ca geothermometer results. An estimate of the geothermal energy using the volumetric method, gave a total geothermal reserve potential of 1.823 MWe.

Keywords: magnetotelluric; geochemistry; geothermal; Blawan; reservoir

1. Introduction

Indonesia contains about 40% of the global geothermal potential with about 80% of it being volcano-hosted geothermal, as Indonesia has 127 volcanoes—or about 13% of volcanoes around the globe [1–3]. There are 265 identified geothermal energy locations with a total potential of 28.1 GWe. Most of the potential is associated with volcanic lines, which generally has high enthalpy, and can be commercially developed for power generation. A small portion of geothermal sources are associated with non-volcanic systems, and usually have a relatively low temperature reservoir. Geothermal systems in Indonesia can generally be divided into five types based on the geological structure which is a predictor for the magnitude of its potential: volcano complexes and graben—caldera volcanic cones—generally have a potential energy that is much larger than the other types. So far, only about 4% of geothermal energy are optimally used in Indonesia. Furthermore, there is few resources available for the study, research, and community education of volcanoes and geothermal energy.

Indonesia has about 265 existing geothermal areas with 138 locations (52.07%) of those existing geothermal areas still at the initial stage of preliminary investigation to inventory their potential

resource class, while 24 other locations (9.05%) are still at the stage of introduction investigation to the potential of the resource class hypothetical. Only seven geothermal locations, or 2.64%, are currently utilized for electricity generation with a total installed capacity of 1189 MW.

Some of undeveloped geothermal area commonly directly used by the local community for tourism, heating, mushroom crops, fertilizer production, agricultural industry, and fish farming. However, in general the direct use of geothermal in Indonesia have not been developed [4].

The Ijen volcano is one of the most active volcanoes—located in eastern of Java, Indonesia—and it is known for its large hyper acidic crater lake. The Ijen volcano presents significant volcanic and environmental hazards to its immediate surroundings. Besides its threats, the volcano provides some benefits for the surrounding people through sulfur mining, tourism, and geothermal energy. In Blawan village north of the Ijen volcano, there are about 21 hot springs with surface temperatures ranging from 40 to 55 °C. This means the Ijen volcano complex, especially at Blawan area, is of significant interest for development as a geothermal field. In addition, the Blawan–Ijen volcano complex also has high potential for agriculture for primary commodities such as coffee, timber, and fruits. Furthermore, lush natural conditions in the caldera of old Ijen are home to residents with the establishment of the Sempol district in Bondowoso [5].

2. Geological Settings

The Ijen caldera was formed more than 50,000 years ago as a result of the collapse of the Ijen stratovolcano [6]. The Ijen caldera has diameter of ± 15 km to the caldera wall and has a high elevation in the northern region, curving to the southern region (Figure 1). The highest point of Ijen caldera complex is in the south-eastern side, which is the peak of Mt. Merapi with an elevation of 2600 meters above sea level (Figure 1). In the northern part of the caldera, the caldera wall forms a steep-slope with an elevation of 850 (near Blawan village) to 1558 m above sea level [7]. The southern region is mostly covered by volcanic deposits from the eruption of post-caldera volcanic cones [8].

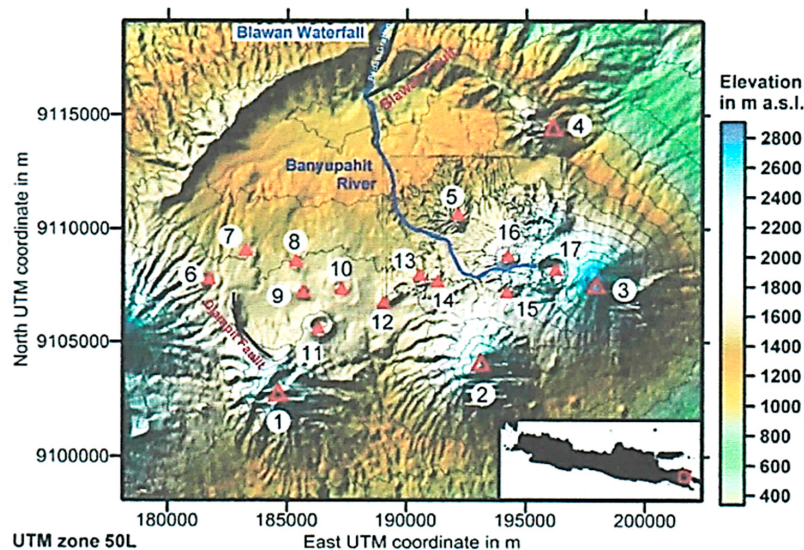


Figure 1. Digital elevation model of the Ijen caldera complex. Red triangles indicate post-caldera volcanoes: 1: Jampit; 2: Ranteh; 3: Merapi; 4: Ringgih; 5: Blau; 6: Cemara; 7: Melaten; 8: Lingker; 9: Anyar; 10: Genteng; 11: Pendil; 12: Gelawan; 13: Kukusan; 14: Telaga Weru; 15: Widodaren; 16: Papak; 17: Kawah Ijen [9].

The Ijen caldera complex was formed in the Pleistocene era along with the formation of two other volcanic centers in Java Island—Mt. Tengger and Mt. Ijang. The evolution of the Ijen caldera complex is divided into three periods as follows [10]:

- Pre-caldera period. This period occurred around $0.29 \text{ Ma} \pm 0.003$, resulting in a huge stratovolcano. Sequences of layers were pyroclastic flows, pyroclastic fallout deposits, and basaltic flows. Dacite lava flows can be found in the northern side of the caldera rim. Outcrops also can be found at the outside of the southern rim of the caldera, near Songgong village.
- Ijen caldera period. The main process of this period is thought to have occurred between 300,000 and 50,000 years ago. The resulting deposit can be found both inside and outside of the caldera as a thick layer of fall pumice and pumice of pyroclastic flows. At the rim of the caldera, sediment thickness reaches about 100–150 m.
- Post-caldera period. This period is divided into five different periods as follows:
 1. First period—Post-caldera formation, a lake was established within the caldera. Sediment layers formed in the north–north-east regions of the caldera as interbedded volcanoclastic shales, silts, and lahar were deposited. The presence of volcanic ash shows that the lake was formed during the reactivation process of volcanic activity inside the caldera [10].
 2. Second period—Consists of volcanic activity inside the caldera and the growth of the lava dome of Mt. Blau [10].
 3. Third period—This period is characterized by the growth of four volcanoes: Mt. Ringgih, Mt. Jampit, Mt. Ranteh, and Mt. Merapi. The volcanic products vary in chemical composition from basalt to andesite. Fall pumice, pyroclastic flows, lahar, and lahar flows can also be found [11]. Three of the four volcanoes (Mt. Jampit, Mt. Ranteh, and Mt. Merapi) lie along the southern edge of the caldera which suggests a significant fault linked to the formation of the caldera and shallow magma chamber. The sequence also follows a tectonic lineament associated with fault structures. Petrologic studies show that Blau (resurgent dome) and the four volcanoes above are associated with the other magma bodies from the pre-caldera formation period [12].
 4. Fourth period—About 50,000 years ago, the lake was emptied through the northern part of caldera. Based on existing stratigraphy, drainage of the lake occurred in two different occasions.
 5. Fifth period—This last period occurred about 25,000 years ago and consisted of the formation of 12 cinder cones in a line oriented east to west. This trend appears to be more or less parallel to the tectonic lineament [13] and shows the migration of volcanic activity from west to east across the caldera. The youngest part of this cinder cone is the Ijen Crater [12].

Volcanic acitivity of Mt. Kendeng totally stopped after the formation of Ijen caldera and some faults in the caldera wall. Pedati fault was formed in northern part of caldera wall, while Jampit fault was formed in the southwest. The processes of erosion and sedimentation of volcanic materials took place after the formation of the caldera. Some loose pyroclastic material formed lahars which were then deposited on low lying areas. The lahar deposits that hardened are impermeable, so water accumulated in the Ijen caldera, forming Lake Blawan. Erosion and sedimentation processes take place continuously both inside and outside caldera. Erosion outside the caldera removed both loose material as well as hard ignimbrite deposits. The loose material was deposited in the Madura Strait and Bali Strait. Meanwhile, erosional material from inside the caldera was transported and deposited in Lake Blawan and formed a lake clastic sediment. It is dominated by smooth volcanic material that forms sandstone and siltstone [14].

Erosion takes place where the greywacke zone in the Pedati fault is reached by the water surface of Lake Blawan. Water flows across the Pedati fault towards Madura Strait, leading to focused erosion within the fault which eventually erodes down to the level of the lake floor. The existence of a way out for the water through the fault causes Lake Blawan to become dry. The lake sediment clastic layers near Kali Sat, Kali Sengon, and Banyupait River are also eroded again forming deep valleys. This process lasted for a long period and was accompanied by lithification of lake clastic sediments. Large tectonic events caused the formation of some faults in the area, such as Blawan fault, Watucapil fault, and Kukusan fault, oriented from northeast to southwest and there is also the possibility of hidden faults oriented from east to west in the southern part of the Ijen caldera. Tectonic events are suspected to

be triggers of volcanic activity in the post-caldera era. Centers of post-caldera volcanic eruptions are located in the weak zone aligned east–west starting from Mt. Merapi and Mt. Ijen in the eastern region to Mt. Raung in the western region [14].

3. Materials and Methods

We have conducted field experiments in the Blawan area on the north rim of Ijen caldera. The Blawan area is a caldera lake sitting on volcanic deposits with an abundance of pumice which formed sandstone and silt. The presence of geothermal potential at this location is characterized by hot springs scattered in the north of the area [14]. Various geophysics investigations have been carried out in Blawan since 2013 to understand the geothermal characteristics and resources in the area. Those geophysical studies were limited to the shallow portion of the region. Shallow resistivity surveys were conducted to determine the distribution of hot water [8]. Other geophysical surveys—like gravitational [15] and magnetic [16]—also provided valuable information about the shallow geothermal zone.

We performed a magnetotelluric survey from 21 February to 12 March, 2015 using a Metronix ADU-07e manufactured by GmbH (Braunschweig, Germany). The ADU-07e measures two orthogonal components of an electric field (E_x and E_y), and three components of the magnetic field (H_x , H_y , H_z). Nineteen MT sites were observed with three magnetic sensors to measure the magnetic horizontal and vertical field and two 30 m long dipoles with electrodes oriented N–S and E–W to measure the electric field (Figure 2). The frequencies used during the study ranged from 0.01 Hz to 10,000 Hz. The observed data, which were stored in the ADU-07e database, were immediately downloaded to a personal computer upon arrival at the field base. The downloaded data were transformed for processing, and three frequency band data sets were generated at different sampling rates. For the high frequency (HF) band, 65 kHz sampling was selected. For the mid frequency (MF) and the low frequency (LF) bands, the sampling rates were set to 4 kHz and 128 Hz, respectively.

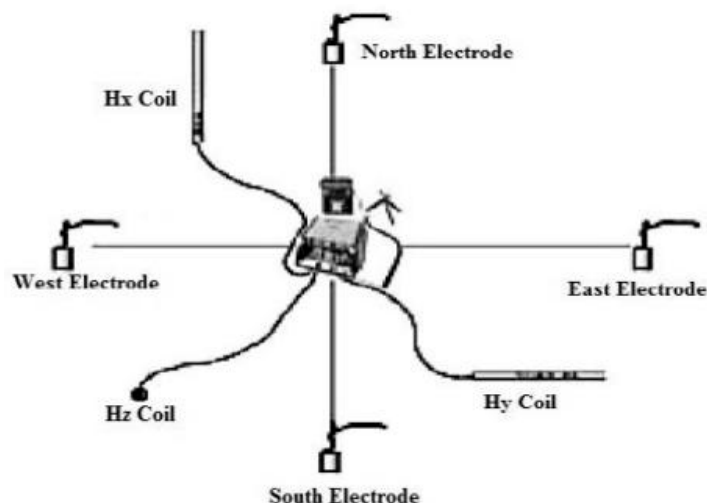


Figure 2. The configuration for the magnetotelluric acquisition used four porous pots (2 for E_x and 2 for E_y) and three magnetic coils (H_x , H_y , and H_z) that were set in different quadrants so that each coil could record the orthogonal x, y, and z magnetic components.

The configuration of the site locations was based on the structure and geological characteristics of the area. The geometry of the sites was designed to be approximately rectangular (Figure 3). In general, the sites were approximately 250 m to 1200 m apart depending on access constraints, but around the hot springs, the sampling distances were shorter to in order to characterize the hot springs well.

We also sampled the hot spring water for geochemical analyses. There were six sampling sites (Figure 3). Acidification of the cation aliquots to prevent scaling after sampling was done, and

spectrophotometry (UV-VIS and AAS, Shimadzu, Kyoto, Japan) was used to analyze the anion and cation concentrations (Table 1). This AAS method is a common method used to measure the cations in water in relatively low concentrations. Elemental analysis of Cl^- , SO_4^{2-} , and HCO_3^- was used to determine the type of water, which is characterized based on its dominant elements: it can be chloride water, sulfuric acid, or bicarbonate. Meanwhile, elemental analysis of SiO_2 , Na^+ , K^+ , Ca^+ , and Al was used to determine the reservoir temperature. The temperature was calculated using the appropriate geothermometer for the dominant elements.

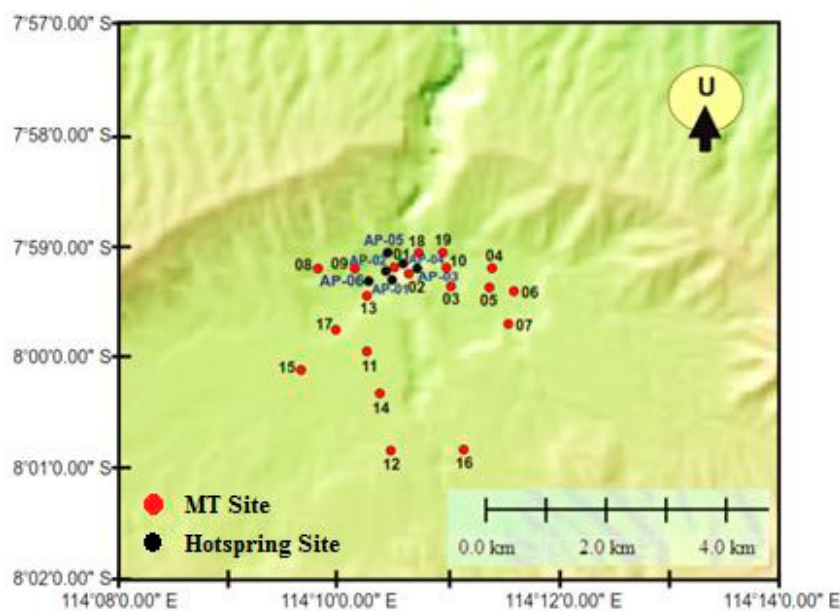


Figure 3. Magnetotelluric points of survey are marked by red dots spread out surrounding hot spring sites (black dots).

Table 1. Geochemical Test Method

Elements	Test Method
Cl	UV-VIS
HCO_3^-	UV-VIS
SO_4^{2-}	UV-VIS
SiO_2	AAS
Na	AAS
K	AAS
Ca	AAS
Al	AAS

All the magnetotelluric data were processed using the MAPROS (Metronix, Braunschweig, Germany) software package. The fields are measured in the time domain and are transformed into the frequency domain where cross-spectra are computed, and from these spectra, the MT response function estimates are derived. Horizontal field components are related by the complex MT impedance tensor. For two-dimensional analysis, the measurement axes are rotated to maximize $|Z_{xy}|^2 + |Z_{yx}|^2$, thereby the diagonal impedance elements Z_{xx} and Z_{yy} are zero while principal impedances Z_{xy} and Z_{yx} represent the two independent transverse magnetic (TM) and transverse electric (TE) modes of polarizations [17,18]. The TM mode is defined as having an electric field across strike direction while the TE mode has the electric field parallel to strike. The TE and TM mode apparent resistivities (ρ), and phases (Φ) are derived from the off-diagonal elements of the impedance tensor.

4. Results

4.1. Magnetotelluric Analysis

The data were inverted for 2D conductivity models in WinGlink (Schlumberger, Houston, TX, USA). Both data modes (i.e., electric and magnetic transverse) were used during the inversion process to obtain the model. The 19 magnetotelluric sites were divided in to four profile inversions (Figure 4). A regularized solution to the MT inverse problem for finding the model \mathbf{m} that minimizes the objective function $S(m)$ is given by [19]

$$S(m) = (d - F(m))^T \hat{R}_{dd}^{-1} (d - F(m)) + \tau |L(m - m_o)|^2 \quad (1)$$

where d is the observed data vector, F is the forward modelling operator, m is the unknown model vector, \hat{R}_{dd} is the error covariance matrix, L is a linear operator, m_o is the reference model, and τ is the user defined regularization parameter. In Equation 1, the first term on the right-hand side represents the data misfit and the second term quantifies the acceptability of the model and can be controlled by changing the regularization parameter τ [20].

The data misfit and model smoothness were analyzed to set up the regularization parameter (τ) for each profile. Testing values from 0.1 to 100 gave the best fit for $\tau = 3$. An error of 20% for the apparent resistivity and 10% for the phase were assigned based on data misfits. A final model was chosen that balanced the requirements for a spatially smooth model with an acceptably small data misfit.

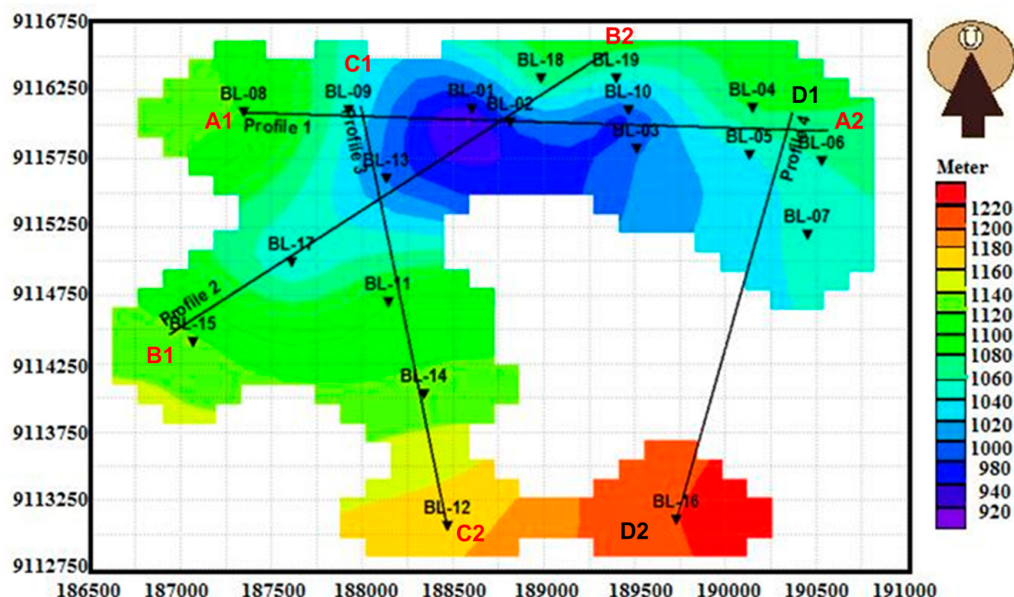


Figure 4. The 19 magnetotelluric points were divided into four inversion profiles to ease interpretation with the locations projected onto the profile lines.

Our final 2D models created using WinGlink, developed by Schlumberger, along profile A1–A2, profile B1–B2, profile C1–C2, and profile D1–D2 are shown in in Figure 5. The 2D model of profile A1–A2 (Figure 5a) achieved a normalized r.m.s. (root mean square) misfit of 4.455% after 136 iterations. The 2D model of profile B1–B2 (Figure 5b) achieved a normalized r.m.s. (root mean square) misfit of 3.005% after 152 iterations. The 2D models of profile C1–C2 shown in (Figure 5c) achieved a normalized r.m.s misfit of 3.788% after 154 iterations. Finally, Figure 5d presents the 2D model of profile D1–D2 which achieved a normalized r.m.s. misfit of 1.967% after 164 iterations.

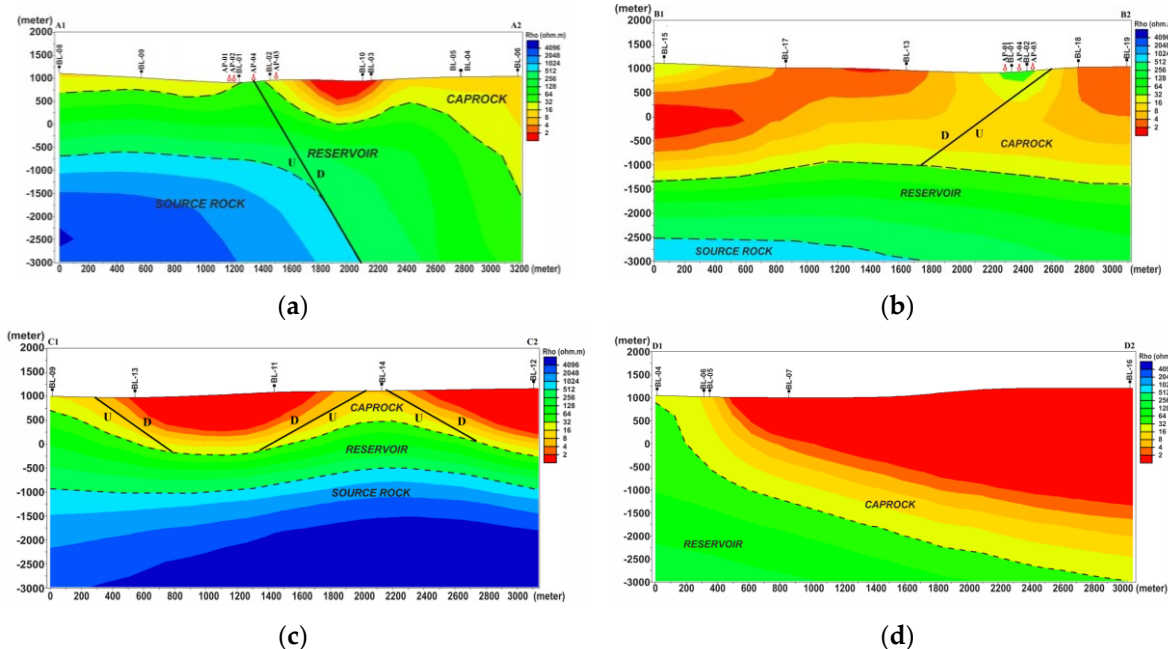


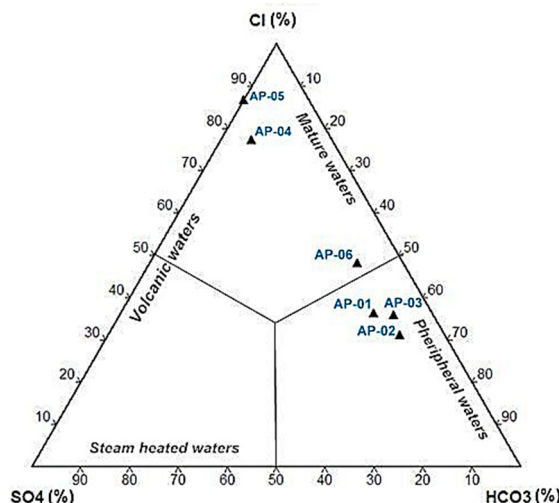
Figure 5. 2D models of (a) profile A1–A2 identified a low resistivity zone ($<32 \Omega\text{m}$) extending to a depth of 750 m above sea level which thickened to the west, and is indicative of hydrothermal alteration processes. This profile also indicated that the Blawan fault allowed fluid migration. Profile B1–B2 (b) is through a zone composed of pyroclastic fall deposits and found low resistivity values. The 2500 m thick low resistivity value zone is a weak zone that is associated with the lineament of the Blawan fault. Profile C1–C2 (c) is composed of sediment deposits from Lake Blawan and also has low resistivity zone indicative of hydrothermal alteration processes. A high resistivity zone was located in the west side at depths from 1000–3000 m below sea level. No lineament was found in this profile. Profile D1–D2 (d) shows the low resistivity zone is very thick and get thicker towards BL-16. It is associated with Pleistocene sediment deposit from Lake Blawan and the Kalisengon River as well as with the volcanic activity of Mt. Blau.

4.2. Geochemical Analysis

We used water geochemical data as supporting data. Analysis of the hot springs water are shown in Table 2. From the six samples taken, we obtained water pH ranges of 6 to 7. Since all of samples have pH close to neutral ($\text{pH} = 8$), we concluded that the Blawan hot springs are eligible to be used as representative samples to characterize the geothermal reservoir. Figure 6 shows the constructed ternary ($\text{Cl}-\text{SO}_4-\text{HCO}_3$) diagram for the Blawan hot springs. This diagram is used to indicate the characteristic type of geothermal water and subsurface geothermal conditions at which the dissolved ions in the surface ascending thermal fluids originate [21]. The ternary diagrams illustrate that the water types of the hot springs are bicarbonate water (AP-01, AP-02, and AP-03) and chloride water (AP-04, AP-05, and AP-06). The high levels of HCO_3 found in Blawan springs probably resulted from mixing of surface groundwater with CO_2 rich steam which boiled off the hydrothermal system [22–24]. Meanwhile, the high Cl concentrations are derived from the reservoir and indicate a permeable zone in this area. The low-Na concentration are caused by mixing hot water with surface water, so the temperature of the hot water sample is reduced.

Table 2. Geochemical analysis

Parameter	Concentration (mg/kg)					
	AP-01	AP-02	AP-03	AP-04	AP-05	AP-06
pH	6.628	6.718	6.648	6.822	7.685	6.725
Cl	130	145	140	160	130	150
HCO ₃	187.44	280.28	220	13.2	0	132.88
SO ₄	43.908	43.731	32.594	34.678	20.222	29.792
SiO ₂	13.43	12.25	9.72	15.29	9.06	10.62
Na	0.016	0.017	0.01	0.012	0.014	0.018
K	46.86	18.53	35.65	30.08	72.7	57.03
Ca	6.614	6.301	6.668	6.638	3.446	5.576
Al	0	<0.1006	0	0	0	0

**Figure 6.** Ternary diagram of Cl-SO₄-HCO₃ for the Blawan hotspring sites [21].

5. Discussion

The main requirements for the formation of a geothermal system (hydrothermal) are a major source of heat, a reservoir to accumulate heat, and caprock [25]. The discovery of the faults shown in Figure 5 will support the geothermal system of Blawan, as faults play important roles as pathways and storage for hydrothermal fluids [26]. The distribution of Blawan geothermal system is presented in Figure 7.

Based on the correlation with the geological map of research area (Figure 8), it can be interpreted that the low resistivity zone ($\leq 32 \Omega \cdot m$) is probably composed of sandstone, Blawan lake sediments, and pyroclastic deposits such as volcanic ash. The low resistivity zone dominates to depths of 750 m below sea level and thickens toward the west (spread out along A1–A2). In Profile 2 (spread out along B1–B2), the low resistivity zone dominates from the surface to a depth of 1250 m below sea level. This corresponds to the geological map (Figure 8) that shows the presence of the Blawan fault. For Profile 3 (C1–C2) the low resistivity zone is significantly shallower than in Profiles 1 and 2, and extends from the surface to a depth of 250 m. In Profile 4 (D1–D4) the low resistivity zone thickens towards point BL-16 (in the south) to a depth of 1000 m below sea level. Low resistivity is often associated with hydrothermal alteration processes, and resistivity decreases proportionately with the abundance of clay minerals. In general, the conductive clay products of hydrothermal alteration, and the high temperature associated with geothermal activity tend to result in lower overall resistivity in geothermal systems [27]. We interpret our low resistivity zones as due to caprock with the presence of high clay mineral contents. Caprock is composed of impermeable rocks that prevent hot fluid

in the reservoir being lost to the surface. The low resistivity zone is suspected to be formed in post-caldera period.

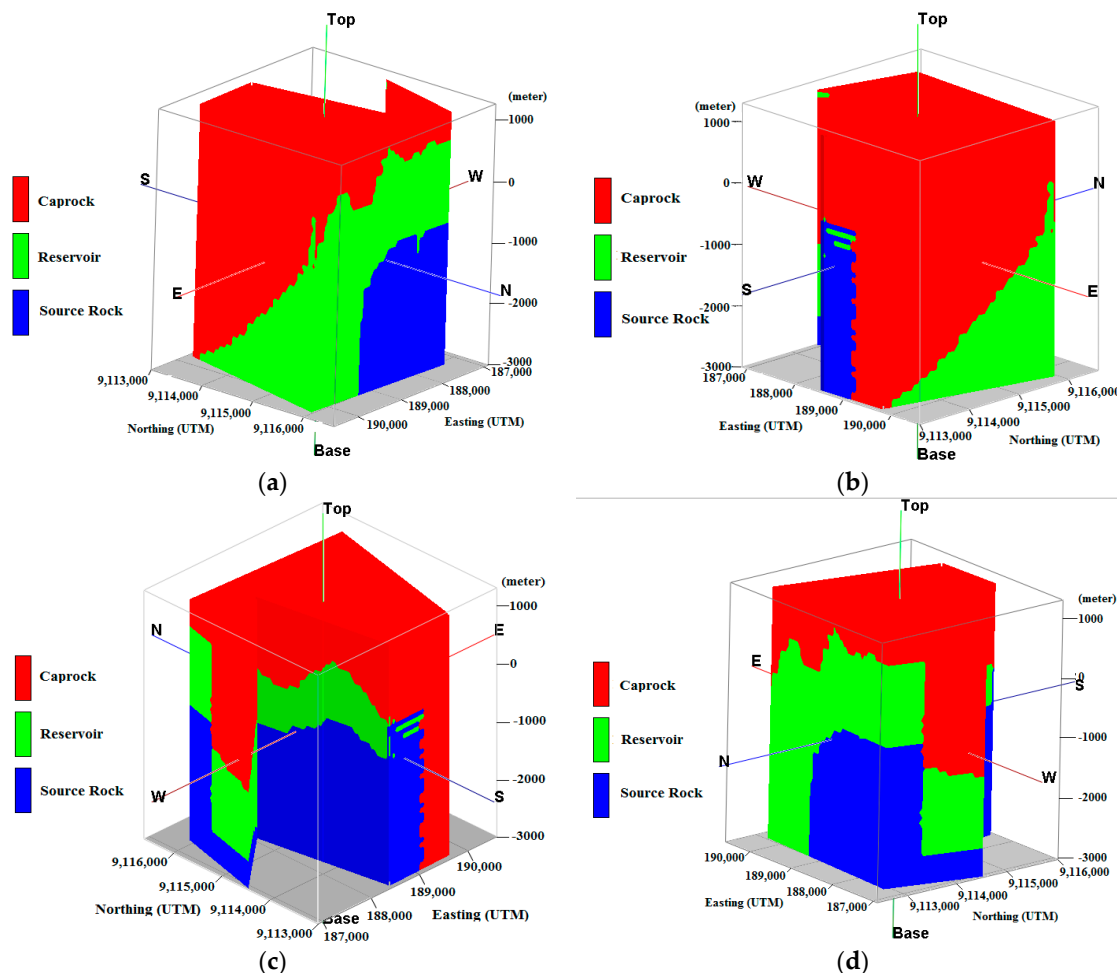


Figure 7. 3D model of the Blawan reservoir showed from (a) north-east, (b) south-east, (c) south-west, and (d) north-west. The low resistivity zone ($\leq 32 \Omega \cdot \text{m}$) covers the surface of the study area and thickens towards east (red zone). A medium resistivity zone ($>32\text{--}\leq 512 \Omega \cdot \text{m}$) is marked in green area and indicates a reservoir where there is accumulation of hot fluid. The blue area is a high resistivity zone ($>512 \Omega \cdot \text{m}$) and it shows indications of the presence of a fault with the orientation of the Blawan fault.

A geothermal reservoir was detected under the caprock in the resistivity range between $>32 \Omega \cdot \text{m}$ and $512 \Omega \cdot \text{m}$ (green zone). The medium resistivity zone spread along A1–A2 (Profile 1) extends in depth from 750 m above sea level to 750 m below sea level and thickens toward the east to a depth of 3000 m below sea level. In Profile 2 (B1–B2), the medium resistivity zone extends from 1250 m to 2500 m below sea level. In Profile 3 (C1–C2), the medium resistivity zone starts at a depth of 250 m below the surface and extends to 1000 m below the sea level. In Profile 4 (D1–D2), the medium resistivity zone thickens toward point BL-04. The higher resistivity of the deep reservoir is thought to reflect the transition in alteration products to less conductive forms at increasing temperatures. The geothermal reservoir is where hydrothermal fluids heated by the heat source, which here means hot rock [28], accumulate. The presence of a fault (Figure 7d) is thought to be an outflow path for the Blawan geothermal system. Based on volumetric analysis from 3D model, the volume of Blawan geothermal reservoir was estimated about $1.65 \times 10^{10} \text{ m}^3$. Meanwhile, the high resistivity zone ($>512 \Omega \cdot \text{m}$) is predicted to be the heat source which supplies the energy to all of the Blawan geothermal system. The high resistivity zone in Profile 1 (spread along A1–A2) was found at a depth of 750 m to 3000 m

below sea level at the western side of profile 1. This zone also indicates a lineament of the Blawan fault which was formed by tectonic processes in the post-caldera period. In Profile 2 (B1–B2) the high-resistivity zone was at depths of 2500 m to 3000 m below sea level at the left side of profile (Figure 5b). While in Profile 3 (C1–C2), this zone extends along the profile from depths of 1000 m to 3000 m below sea level. In Profile 4 there is no high resistivity zone detected.

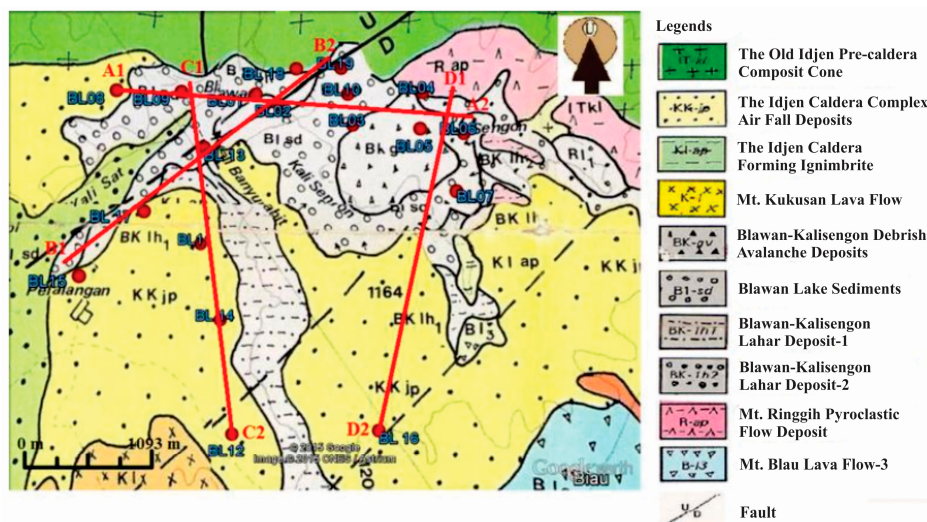


Figure 8. MT acquisition points overlaid with Blawan geological map. Rock formations in the study area are divided into three types. The Ijen Caldera Complex Air Fall Deposits (KKjp) are thought to have resulted from pyroclastic fall deposits from several eruption points (Mt. Blau, Mt. Ijen, Mt. Rante, and Mt. Suket). Blawan Lake Sediment (Bl sd) is characterized as intermediate between shale and sand, and some travertine sediments which contain fossils. The Blawan-Kalisengon avalanche debris deposit is composed of sediment from Lake Blawan and lava flows of Mt. Ringgih and Mt. Blau.

We used a Na–K–Ca geothermometer to determine the reservoir temperature, since this geothermometer is suitable for low enthalpy geothermal system with high Ca and almost no Al content as found at Blawan. This geothermometer has a high accuracy for hot springs that are at medium temperature and not completely in equilibrium as in Blawan. It also gives a low error calculation for unsteady reservoirs. We used the Fournier & Truesdell (1973) Na–K–Ca geothermometer equation [29] (Equation 2 below). Alternative geothermometers, such as the Na–K geothermometer are not suitable for the Blawan hot spring conditions with its high-Ca content and where $\log((\text{Ca}^{0.5}/\text{Na}) + 2.06)$ is positive. The Na–K geothermometer requires a low Ca content and a negative value for $\log((\text{Ca}^{0.5}/\text{Na}) + 2.06)$. Additionally, the Na–K geothermometer is applicable for reservoirs that have temperature ranges from 180 to 350 °C [30].

Because the chloride hot springs are the most representative for determining the reservoir condition [21], we used our chloride water samples from AP-04, AP-05, and AP-06 for our geothermometer analysis. The temperature of the reservoir from which the chloride water was derived is given by

$$T^{\circ}\text{C} = \frac{1647}{\log(\text{Na}/\text{K}) + \beta(\log(\sqrt{\text{Ca}}/\text{Na}) + 2.06) + 2.47} - 273.15 \quad (2)$$

This indicated that our inferred temperature at depth is approximately 90 °C which, according to Hochstein et al. [24], (Table 3), is classified as low temperature [7,21].

An estimate of the geothermal potential energy was carried out to evaluate the possible geothermal capacity of the Blawan geothermal field. Potential energy estimation is based on the volumetric method

in Indonesian National Standard No. 13-6171-1999 [31], assuming the following parameters given in Table 3 [31]. Based on these, the geothermal field is found to be have a potential energy of 1.823 MWe. This magnitude of geothermal resource is considered a promising area, and could be developed as a small power plant or for direct use in the field of agribusiness.

Table 3. Na–K–Ca geothermometer

Sampling Point	Ion	mg/kg	Temperature (°C)
AP-04	Na	0.012	61.15
	K	30.08	
	Ca	6.638	
AP-05	Na	0.014	107.1
	K	72.7	
	Ca	3.446	
AP-06	Na	0.018	89.65
	K	57.03	
	Ca	5.576	

6. Conclusions

The result of magnetotelluric data processing and interpretation shows that the geothermal system in the study area consists of a caprock zone ($\leq 32 \Omega \cdot \text{m}$), reservoir zone ($> 32 \Omega \cdot \text{m}$ to $\leq 512 \Omega \cdot \text{m}$), and a heat source zone ($> 512 \Omega \cdot \text{m}$), and is supported by the presence of a fault. Geochemical analysis shows that the hot springs in the research area consist of bicarbonate water type (AP-01, AP-02, AP-03) and chloride water (AP-04, AP-05, AP-06). A Na–K–Ca geothermometer analysis indicated that the Blawan geothermal reservoir has a temperature of approximately 90 °C which implies a low temperature geothermal system. The potential of Blawan geothermal energy is found to be 1.823 MWe.

Acknowledgments: Authors would like to thank to Partnerships for Enhanced Engagement in Research (PEER) grant from USAID No. PGA 2000005053, Hibah Penguatan Pusat Studi, Research and Community Services Institution, and World Class University program of Universitas Brawijaya for partially financial support. Thanks also given to all people who participated during acquisition in Blawan. We also thank to reviewers who gave many suggestions in improving our manuscript. Their generous contribution of time and expertise are greatly appreciated.

Author Contributions: Sukir Maryanto developed the design survey, obtained funding, and participated. Cinantya N. Dewi collected MT data during acquisition and took samples for geochemical analysis. All authors contributed to data interpretation and final editing.

Conflicts of Interest: The authors declare no conflict of interest. The funding sponsor had no role in the survey design, collecting data, analysis, or data interpretation, in writing of manuscript, or decision to publish the results.

References

- Iguchi, M.; Nishimura, T.; Hendrasto, M.; Rosadi, U.; Ohkura, T.; Triastuty, H.; Basuki, A.; Loeqman, A.; Maryanto, S.; et al. Methods for Eruption Prediction and Hazard Evaluation at Indonesian Volcanoes. *J. Disaster Res.* **2012**, *7*, 26–36.
- Maryanto, S.; Santosa, D.; Mulyana, I.; Hendrasto, M. Preliminary chaos analysis of explosion earthquakes followed by harmonic tremors at Semeru Volcano, East Java, Indonesia. *World Acad. Sci. Eng. Technol.* **2010**, *4*, 612–617.
- Maryanto, S.; Iguchi, M.; Tameguri, T. Constraints on the source mechanism of harmonic tremors based on seismological, ground deformation, and visual observations at Sakurajima volcano, Japan. *J. Volcanol. Geotherm. Res.* **2008**, *170*, 198–217. [[CrossRef](#)]
- Santoso, D.; Maryanto, S.; Nadhir, A. Application of Single MEMS-accelerometer to measure 3-axis vibrations and 2-axis tilt-angle simultaneously. *Telkomnika* **2015**, *13*, 442–450. [[CrossRef](#)]

5. Konstantinuo, K.I.; Perwita, C.A.; Maryanto, S.; Budianto, A.; Hendrasto, M. Maximal Lyapunov exponent variations of volcanic tremor recorded during explosive and effusive activity at Mt. Semeru volcano, Indonesia. *Nonlinear Process. Geophys.* **2013**, *20*, 1137–1145. [[CrossRef](#)]
6. Van Hinsberg, V.; Berlo, K.; van Bergen, M.; Jones, A. Extreme alteration by hyperacidic brines at Kawah Ijen volcano, East Java, Indonesia: I. Textural and mineralogical imprint. *J. Volcanol. Geotherm. Res.* **2010**, *198*, 253–263. [[CrossRef](#)]
7. Van Bergen, M.; Bernard, A.; Sumarti, S.; Sriwana, T.; Sitorus, K. *Crater Lake of Java: Dieng, Kelud, and Ijen. Excursion Guidebook*; IAVCEI General Assembly: Bali, Indonesia, 2000.
8. Karlina, I.; Maryanto, S.; Rachmansyah, A. Distribution of hot springs Blawan-Ijen based on geoelectricity data. *J. Nat. B* **2013**, *2*, 164–171.
9. Mauri, G. Multi-Scale Analysis of Multiparameter Geophysical and Geochemical Data from Active Volcanic Systems. Unpublished Ph.D. Thesis, Simon Fraser University, Burnaby, BC, Canada, 2009.
10. Sitorus, K. Volcanic Stratigraphy and Geochemistry of the Idjen Caldera Complex, East Java, Indonesia. Unpublished MSc Thesis, University of Wellington, Wellington, New Zealand, 1990.
11. Van Hisberg, V. Water-Rock Interaction and Element Fluxes in the Kawah Ijen Hyperacid Crater Lake and the Banyu Pahit River, East Java, Indonesia. Unpublished Master’s Thesis, Utrecht University, Utrecht, The Netherlands, 2001.
12. Berlo, K. The Magmatic Evolution of the Ijen Caldera, East Java, Indonesia. Unpublished Master’s Thesis, Utrecht University, Utrecht, The Netherlands, 2001.
13. Carn, S. Application of Synthetic Aperture Radar (SAR) imagery to volcano mapping in the humid tropics: A case study in East Java, Indonesia. *Bull. Volcanol.* **1999**, *61*, 92–105. [[CrossRef](#)]
14. Zaennudin, A.; Wahyudin, D.; Surmayadi, M.; Kusdinar, E. Hazard assessment of Ijen volcanic eruption East Java. *J. Environ. Geol. Hazard* **2012**, *3*, 109–132.
15. Raehanayati; Maryanto, S.; Rachmansyah, A. Study of Geothermal Potential in Blawan-Ijen, East Java Based On Gravity Method. *J. Neutrino* **2013**, *6*, 31–39. (In Indonesian).
16. Afandi, A.; Maryanto, S.; Rachmansyah, A. Identification of Geothermal Reservoir based on Magnetic Method for Blawan Area, Bondowoso. *J. Neutrino* **2013**, *6*, 1–10. (In Indonesian).
17. Vozoff, K. The Magnetotelluric method. In *Electromagnetic Methods in Applied Geophysics. Volume 2, Application, Parts A and B*; Nabighian, M.N., Ed.; Society of Exploration Geophysicists: Tulsa, OK, USA, 1991; pp. 641–711.
18. Gamble, T.; Gouba, W.; Clarke, J. Magnetotellurics with a remote magnetic reference. *Geophysics* **1979**, *44*, 53–86. [[CrossRef](#)]
19. Tikhonov, A.; Arsenin, V. Solutions of Ill-Posed Problems. John Wiley & Sons: New York, NY, USA, 1977.
20. Xiao, W. Magnetotelluric Exploration in the Rocky Mountain Foothills. Master’s Thesis, University of Alberta, Edmonton, AB, Canada, 2004.
21. Sukhyar, R.; Gurusinga, C.; Widodo, S.; Munandar, A.; Dahlan, H.M.; Wahyuningsih, R. *Potential and Development of Indonesia Geothermal Resources*; Geological Agency of Indonesia: Bandung, Indonesia, 2014. (In Indonesian)
22. Ellis, A.J.; Mahon, W.A. *Chemistry and Geothermal System*; Academic Press: New York, NY, USA, 1977.
23. Delmelle, P.; Bernard, A.; Kusakabe, M.; Fischer, T.; Takano, B. Geochemistry of magmatic-hydrothermal system of Kawah Ijen volcano, East Java, Indonesia. *J. Volcanol. Geotherm. Res.* **2000**, *97*, 31–53. [[CrossRef](#)]
24. Hochstein, M.; Zheng, K.; Pasvanoglu, S.; Vivian-Neal, P. Advective (heat sweep) geothermal systems. In Proceedings of the 38th Workshop on Geothermal Reservoir Engineering, Stanford, CA, USA, 11–13 February 2013.
25. Kasbani. Type of geothermal systems in Indonesia and potential energy estimation. *Bull. Geol. Agency* **2009**, *4*, 64–73.
26. Asaue, H.; Koike, K.; Yoshinaga, T.; Takakura, S. Magnetotelluric resistivity modelling for 3D characterization geothermal reservoir in the Western Side of Mt. Aso, SW Japan. *J. Appl. Geophys.* **2005**, *58*, 296–312.
27. Ussher, G.; Harvey, C.; Johnstone, R.; Anderson, E. Understanding The Resistivities Observed In Geothermal Systems. In Proceedings of the World Geothermal Congress, Kyushu-Tohoku, Japan, May 28–10 June 2000; pp. 1915–1920.
28. Mardiana, U. *Geothermal Manifestation of Papandayan Based on Rock Resistivity Value, Case Study Mt. Garut-West Java*; Department of Geology Padjadjaran University: Bandung, Indonesia, 2007.

29. Fournier, R.O.; Truesdell, A.H. An empirical Na–K–Ca geothermometer for natural waters. *Geochim. Cosmochim. Acta* **1973**, *37*, 1255–1275. [[CrossRef](#)]
30. Ellis, A.J. Chemical Geothermometry in Geothermal Systems. *Geothermics* **1979**, *25*, 219–226. [[CrossRef](#)]
31. National Standardization Agency. *Geothermal Energy Potential Estimation Method*; Indonesian National Standard No. 13-6171-1999; National Standard Agency: Jakarta, Indonesia, 1999; pp. 1–9.



© 2017 by the authors. Licensee MDPI, Basel, Switzerland. This article is an open access article distributed under the terms and conditions of the Creative Commons Attribution (CC BY) license (<http://creativecommons.org/licenses/by/4.0/>).